JMEPEG (2019) 28:5541–5550
https://doi.org/10.1007/s11665-019-04268-9

1059-9495/$19.00

Few-Layers Graphene Film and Copper Surface Morphology for Improved Corrosion Protection of Copper

Sultan Akhtar, Tahar Laoui, Ahmed Ibrahim, A.Madhan Kumar, Junaid Ahmed, and Ihsan-ul-Haq Toor

(Submitted November 8, 2018; in revised form July 8, 2019; published online August 21, 2019)

Graphene has shown excellent corrosion protection of copper (Cu). The corrosion protection of Cu is governed by the characteristics of the deposited graphene and Cu surface morphology underneath. In this work, graphene films (1-2, 4-5 layers) were deposited on Cu using a chemical vapor deposition by changing hydrogen (H_2) concentration during the annealing stage. The chemical structure and surface microstructural features of graphene/Cu were inspected by Raman spectroscopy, scanning electron microscopy, transmission electron microscopy, and atomic force microscopy. The electrochemical corrosion performance of graphene/Cu was studied in 0.5 M sodium chloride solution using potentiodynamic polarization and electrochemical impedance spectroscopic measurements. The 1-2 layers of graphene and rough Cu surface were obtained for low H_2 concentrations (0 and 2.5%), whereas high H_2 concentrations, 20 and 50%, resulted in a smooth Cu surface and 4-5 layers of graphene. Our results showed that Cu with a smooth surface and multilayer graphene film exhibited the best corrosion resistance against electrochemical degradation. Tafel analysis revealed that Cu with 4-5 layers of graphene coating corroded nearly three orders of magnitude slower than the annealed Cu, without graphene coating. The results of this study can be useful for several applications where Cu is in close contact with salt species.

Keywords chemical vapor deposition, graphene layers, copper, surface morphology , corrosion

1. Introduction

Due to its excellent thermal and electrical characteristics, copper (Cu) is a widely used operational material in electronic devices, energy conversion, and heating and cooling exchangers in industries (Ref 1). However, the oxidation of Cu due to its chemical reactive nature is a serious reliability issue in micro/nano-electronics that rendered its applications limited (Ref 2). This problem is more serious when Cu is in close contact with an environment having chloride ions (Ref 3). Therefore, the development of an efficient protective coating is essential against oxidation and corrosion in order to realize a wide range of applications of Cu.

Recently, researchers working in the field of materials science have shown the potential of graphene as a surface protective coating on metals against corrosion species. This corrosion protection behavior of graphene is related to some of its characteristics such as toughness, hydrophobicity, and impermeability to molecules (Ref 4-6), making it a better candidate for an ultrathin protective coating for Cu against marine and saline environment (Ref 7-9). Graphene coating on metals has proven to be a natural diffusion barrier to aqueous corrosion reactants (Ref 5).

Some researchers reported that graphene could efficiently protect Cu against electrochemical degradation in aqueous media (e.g., NaCl and Na_2SO_4) by reducing the corrosion rate significantly compared to bare Cu (Ref 7, 10, 11). In these studies, graphene was deposited on a Cu substrate through chemical vapor deposition (CVD) method. The CVD method is known to produce a large area uniform graphene film on metals (Ref 12, 13). It is worthwhile to mention that the characteristics of graphene can be influenced greatly by CVD parameters, such as gases (argon, hydrogen, and methane), temperature, annealing time, and growth time (Ref 8, 14-20). Our previous study showed that hydrogen concentration during annealing stage affected both graphene characteristics and surface morphology of underneath Cu (Ref 14).

Though a number of corrosion studies were reported after growing graphene on Cu, to the author's knowledge, no systematic study was performed when graphene was grown by CVD method under different hydrogen concentrations during annealing stage. In this paper, we performed a systematic corrosion study on Cu after growing different layers of graphene on it. The graphene was grown by altering hydrogen concentration between 0 and 50% of the total gas flow during the annealing stage in the CVD reactor. The chemical structures of graphene/Cu were analyzed by Raman spectroscopy, and the microstructural features of graphene/Cu surfaces were examined by scanning electron microscopy (-SEM), transmission electron microscopy (TEM), and atomic force microscopy (AFM). The electrochemical corrosion performance of graphene/Cu was studied in sodium chloride

Sultan Akhtar, Department of Physics Research, Institute for Research and Medical Consultations (IRMC), Imam Abdulrahman Bin Faisal University, Dammam 31441, Saudi Arabia; **Tahar Laoui**, Department of Mechanical and Nuclear Engineering, University of Sharjah, Sharjah 27272, United Arab Emirates; **Ahmed Ibrahim**, Department of Mechanical Design and Production Engineering, Zagazig University, Zagazig 44519, Egypt; **A. Madhan Kumar**, Center of Research Excellence in Corrosion, King Fahd University of Petroleum and Minerals, Dhahran 31261, Saudi Arabia; and **Junaid Ahmed** and **Ihsan-ul-Haq Toor**, Department of Mechanical Engineering, King Fahd University of Petroleum and Minerals, Dhahran 31261, Saudi Arabia. Contact e-mails: suakhtar@iau.edu.sa and tlaoui@sharjah.ac.ae.

solution (0.5 M NaCl) using potentiodynamic polarization and electrochemical impedance spectroscopic measurements. The corrosion rates were calculated using Tafel analysis. The obtained results could be useful for several applications where the surface of Cu is in close contact with corrosion species.

2. Experimental Work

2.1 Synthesis of Graphene Films

In this study, graphene films were grown on thin Cu foil (Alfa Aesar No. 13382) using different hydrogen (H_2) concentrations during the annealing stage of the chemical vapor deposition (CVD). A custom-made atmospheric pressure CVD system (First Nano Co. USA) was used for growing graphene and annealing of Cu specimen (reference sample). A standard CVD cycle includes four main steps in the following order: (1) preheating, (2) annealing, (3) growth, and (4) cooling. Notably, to study the effect of H_2 on graphene and Cu characteristics and hence on corrosion properties of Cu, the concentration of H_2 was varied during step 2 (annealing step) only, while the ratio of H_2 and argon (Ar) was kept constant (37:1463) during steps 1 and 4 for all runs.

At first, Cu foil with dimensions 1×4 cm^2 was heated (from room temperature to 1000 °C) in Ar and H_2 gas mixture environment with a total flow rate of 1500 sccm. In the second step, Cu foil was annealed at 1000 °C for 30 min under H_2 concentrations of 0, 2.5, 20, and 50 vol.% of the total gas mixture. Graphene was grown during the growth process by flowing methane gas into the system chamber for 3 min with a flow rate of 5 sccm. Graphene/Cu specimens were then cooled down to room temperature to complete the CVD process under H_2 and Ar gas mixture (37:1463). The details of the CVD method are reported elsewhere (Ref 14). Depending on H_2 concentration (0, 2.5, 20 and 50%H_2), the graphene samples were denoted as G-Ann-0%H_2, G-Ann-2.5%H_2, G-Ann-20%H_2, and G-Ann-50%H_2. The reference Cu sample with no graphene (annealed Cu) is labelled as Ann-Cu.

2.2 Characterization of Graphene Films

After synthesis, annealed Cu in the CVD chamber without growth (Ann-Cu) and G/Cu specimens were tested for corrosion using potentiodynamic polarization experiment. The morphological characteristics of the as-grown graphene coatings were analyzed by field-emission scanning electron microscopy (FE-SEM) (TSCAN-MIRA 3 LM-USA), and TEM (JEM-2100F, Japan) and AFM (Dimension Icon-Bruker). The structural analysis was carried out by Raman spectroscopy with laser wavelength of 455 nm and optical microscope (DXR™ Raman Microscope, Thermo Scientific, USA). For TEM examination, graphene flakes were transferred onto TEM grids having holey carbon support film after etching the underneath Cu substrate. The SEM and TEM instruments were used at accelerating voltage of 5 and 200 kV, respectively.

2.3 Electrochemical Tests of Graphene/Cu Specimens

The specimens were tested for corrosion in a three-electrode cell assembly in the following order: (1) Cu specimens, (2) platinum wire and (3) a saturated calomel electrode (SCE) acting as a reference electrode. The electrochemical corrosion experiments were completed by exposing an area of 0.2 cm^2 of the specimen in 0.5 M sodium chloride (NaCl) solution. The corrosion data were collected using Gamry Reference 3000 Potentiostat electrochemical workstation. Potentiodynamic polarization (PD) tests were carried out at $\pm$ 250 mV with respect to open-circuit potential with a scan rate of 0.2 mV per second. Corrosion parameters were obtained by analyzing the Tafel regions by applying DC105 corrosion software. Electrochemical impedance spectroscopy (EIS) experiments were performed in the frequency region of 0.10-100,000 Hz with a signal amplitude of 0.10 V. In order to verify the reproducibility of the obtained results, the electrochemical tests were repeated at least three times. The Echem Analyst software was employed to study the EIS results.

3. Results and Discussion

3.1 Morphological Analysis of Graphene/Cu Specimens

To study the corrosion behavior of Cu, different types of graphene films were grown on Cu substrate by altering the H_2 concentration during annealing stage in the CVD reactor. Since during the wet corrosion tests the surface of the specimen makes close contact with a solution, it is crucial to evaluate the surface morphology of the G/Cu specimens prior to any tests. The surface morphological features and the thickness variation of the graphene/Cu were characterized using SEM and AFM (Fig. 1). The electron micrographs of the G/Cu specimens show the different types of deposited graphene (Fig. 1a, b, c, and d). The change of contrast throughout the electron image reflects the thickness variation in the film. The dark regions on a bright background are the small graphene flakes, denoted here as graphene domains. Interestingly, these domains were observed on all specimens; however, they were varied in size, density, and thickness. For example, thicker and large-sized graphene domains were observed for G-Ann-20%H_2 and G-Ann-50%H_2 specimens (Fig. 1c and d). By seeing the dark contrast of the domains, they are relatively thicker than the domains of remaining two specimens, G-Ann-0%H_2, and G-Ann-2.5%H_2. The deposition of large-sized and irregular-shaped multilayer graphene domains in case of higher H_2 is attributed to disassociation of high amount of CH_4 gas (used as carbon source) and the presence of high-density nucleation sites (Ref 15).

Further to graphene morphology, Cu exhibits a high density of steps on its surface when it was annealed under 0%H_2 condition as depicted clearly by AFM (Fig. 1e). These Cu steps can cause extrinsic defects in graphene films and affect the continuity of the deposited graphene around these features (Ref 14, 15). Remarkably, the height of the steps was reduced significantly when Cu was annealed under high H_2 concentration (Fig. 1h), consistent with earlier work (Ref 16). AFM results revealed that Cu surface became smoother by increasing H_2 amount during annealing. The root-mean-square (RMS) value was reduced to 3.6 nm (G-Ann-50%H_2) from around 12.6 nm (G-Ann-0%H_2). Instead of steps, the surface of Cu annealed under high H_2 exhibited bigger particles (Fig. 1g and h) compared to G-Ann-0%H_2; more details on this aspect are reported elsewhere (Ref 14, 15). It should be noted that the surface of the as-received Cu foil often shows high surface roughness due to the presence of strain lines (rolling lines) and

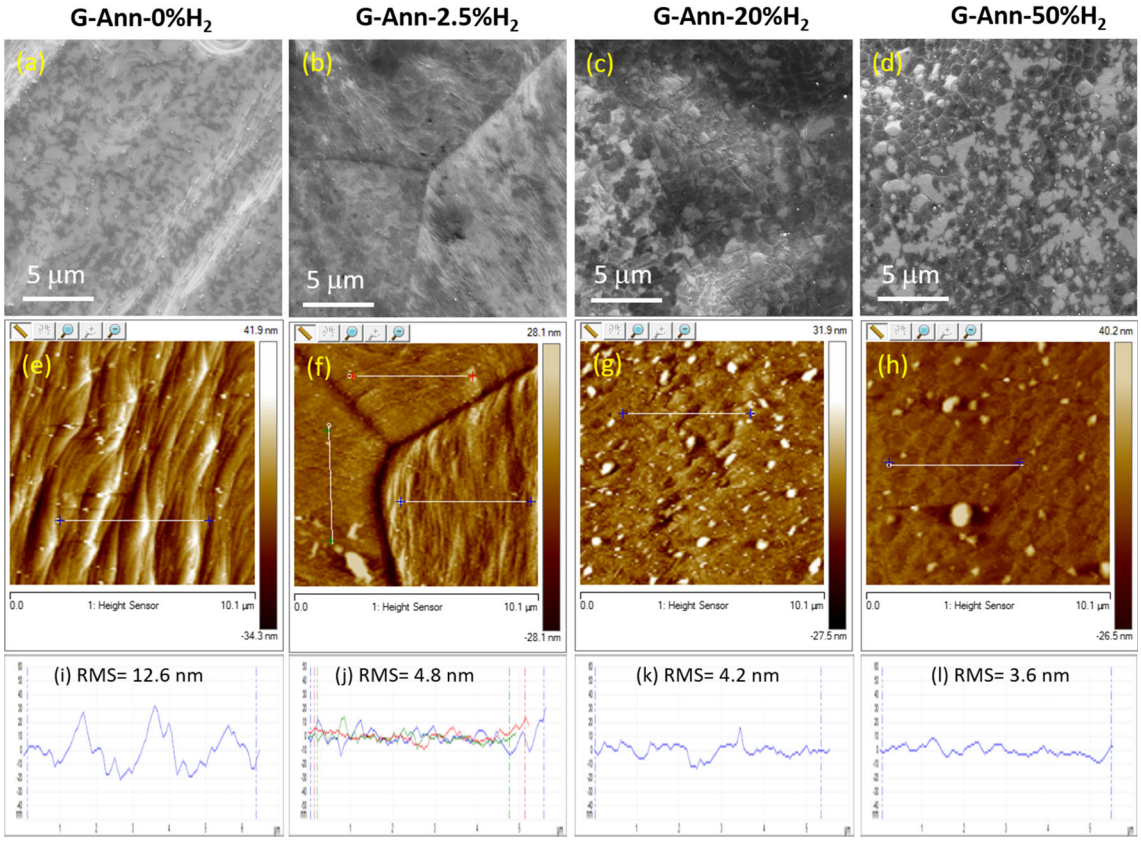

Fig. 1 Morphology of graphene films over Cu substrate. SEM images of G/Cu specimens annealed at different H_2 concentrations (a–d). AFM micrographs of G/Cu specimens (e–h) along with their roughness profiles (i–l). The roughness profile was taken from the area as marked with a line in each case (avoiding grain boundaries and particles to extract roughness information only). Note: The value of RMS was reduced from 12.6 to 3.6 nm with increasing H_2 concentration

grain boundaries. These surface features are diminished to some extent when Cu is annealed under different H_2 conditions during the CVD process. A step-like structure is formed instead if Cu is annealed without H_2 due to oxygen impurities present in the Cu foil as a result of Cu reconstruction (Ref 21). On the other hand, Cu surface becomes smooth and flat when annealed under H_2 due to a reduction effect of rolling lines. This kind of surface could be beneficial for the growth of a uniform layer of graphene and hence gives better surface coverage. From SEM and AFM analyses, it is concluded that H_2 plays an important role in defining the surface morphology of Cu and subsequently the growth of graphene.

The growth mechanism of graphene under different H_2 concentrations is elaborated in detail elsewhere (Ref 14, 22, 23); herein, a summary of this mechanism is provided. For low H_2 (0 and 2.5%H_2), the surface-active sites, *e.g.,* impurity particles, Cu steps, and rolling lines are oxidized and passivated and hence resulted in fewer nucleation sites. Due to the availability of fewer surface-bound active H_2 atoms (-H_2*), less adsorption and dissociation of methane takes place. The presence of fewer C atoms for nucleation points results in slow growth rate of graphene. For higher H_2 (20 and 50%H_2), the surface of Cu is very active leading to an increase in the density of -H_2*, causing stronger adsorption and dissociation of methane (presence of more carbon) along with a high density of nucleation sites. Consequently, the growth rate of graphene is high yielding to the formation of multilayer graphene.

3.2 Structural Analysis of Graphene Films

The thickness and structural information of graphene film on Cu were analyzed by Raman spectroscopy, as shown in Fig. 2a. The graphene films are displaying G (1570-1600 cm^{-1}), 2D (2690-2740 cm^{-1}) and D (1350-1370 cm^{-1}) bands, the characteristics of graphene with minor defects. The intensity ratios of 2D- and G-bands are estimated higher than 1 ($I_{2D}/I_G \approx 1.5$) for G-Ann-0%H_2 and G-Ann-2.5%H_2 specimens suggesting growth of mono/bilayer graphene films (Ref 14, 17). In contrast, multilayer graphene films were identified for G-Ann-20%H_2 and G-Ann-50%H_2 when a higher amount of H_2 was used as judged by I_{2D}/I_G ratio (≈ 0.7), being less than 1 for multilayer graphene (Ref 11, 24). Moreover, it was noted that the graphene films grown under high H_2 concentration displayed a rather high D-band, suggesting presence of defects in these films. It is known that D-band is originated due to several factors, and formation of high-density multilayer graphene domains in the current case could be one of them (Ref 18, 25, 26). Raman spectroscopy results suggested that annealing Cu under Ar or low-pressure H_2 content produced fewer layers graphene as compared to the excessive amount of H_2. These results are consistent with earlier works (Ref 18, 19).

Graphene film of G-Ann-20%H_2 specimen was further analyzed by TEM (Fig. 2b and c). Figure 2b is a typical TEM image of graphene over holey carbon film. A high-resolution image of a graphene edge is displayed in (Fig. 2c), showing 4-5 layers of graphene with a constant distance of around

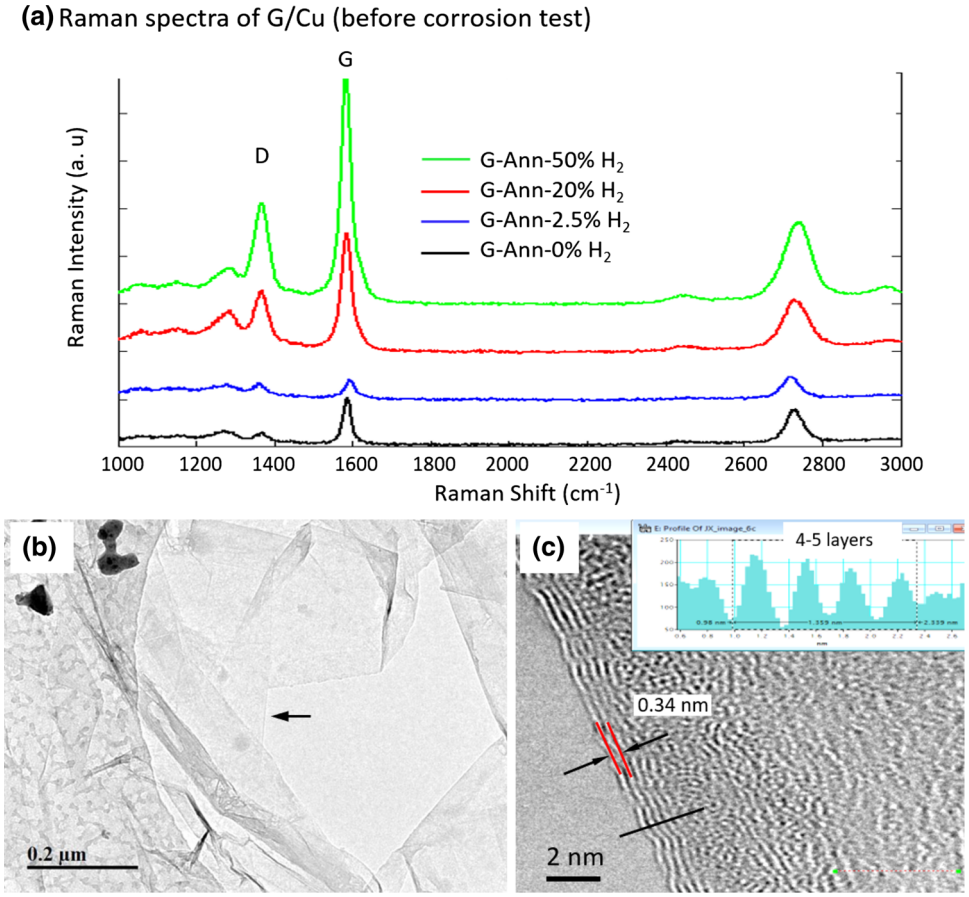

Fig. 2 Structural analyses of graphene films using Raman spectroscopy and TEM. (a) Raman spectra of G/Cu samples showing the characteristic bands, 2D and G of graphene film, and D-band basically displaying the density of multilayer graphene domains. (b) A typical TEM image of graphene over a holey carbon film (G-Ann-20%H_2 specimen was considered for TEM). (c) HR-TEM of the graphene taken from the area as marked with a black arrow in b. Inset is the intensity profile taken from the area highlighted by a black line showing 4-5 layers of graphene

0.34 nm, corresponds to the distance between any two graphene layers (Ref 27, 28). Indeed, TEM analysis supports the Raman results presented in Fig. 2(a), confirming that G-Ann-20%H_2 specimen has multilayer graphene film.

In summary, SEM, AFM, and Raman results have demonstrated that hydrogen concentration during annealing stage has influenced the characteristics of grown graphene in terms of film thickness, and uniformity, as well as surface morphology of Cu. A high H_2 concentration during annealing promotes high density of multilayer graphene domains on a uniform graphene film, while a low amount of H_2 exhibits fewer domains. A thicker graphene film can be obtained on a smooth surface if the Cu is annealed under high H_2 concentration.

3.3 Electrochemical Corrosion Analysis of Graphene/Cu Specimens

Figure 3(a) displays the potentiodynamic polarization (PDP) response of annealed Cu and graphene-coated Cu specimens. In *PDP* curves, it was observed that the corrosion current density (i_{corr}) of the G-Ann-0%H_2 specimen was lower than that of annealed Cu, suggesting that the graphene coating on Cu decreased Cu dissolution. Another observation was the increase in corrosion potential (E_{corr}) of graphene-coated specimen. E_{corr} of the G-Ann-0%H_2 specimen was 53 mV more positive compared to the annealed Cu. The shift in E_{corr} toward noble

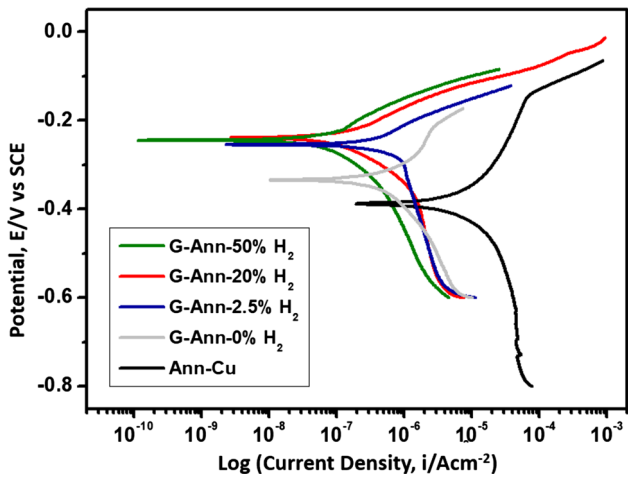

Fig. 3 Corrosion study of Cu substrates. Potentiodynamic polarization (PDP) response of annealed Cu and graphene-coated Cu specimens exposed in 0.5 M NaCl solution at room temperature

direction means an increase in corrosion resistance due to graphene coating. The obtained corrosion behavior of graphene coating on Cu is consistent with earlier work reported by Sing Raman et al. (Ref 10).

For G-Ann-2.5%H_2 specimen (blue curve), E_{corr} increased compared to G-Ann-0%H_2 specimen, and cathodic reaction rate also decreased. This means that the addition of graphene contributed to the decrease in both the cathodic and anodic reaction rates simultaneously. Similar behavior was observed for other specimens, such as G-Ann-20%H_2 and G-Ann-50%H_2; however, the effect was predominant for this Cu (see red and green curves in Fig. 3a). Some previous work also reported this kind of behavior of graphene-coated specimens. For instance, Kirkland et al. (Ref 7) deposited graphene film on Ni and Cu and showed that the films behaved differently on these two substrates. For Ni, graphene mainly inhibited the anodic dissolution of Ni, while the effect was more significant on the cathodic reaction rates in Cu. However, in both cases, the corrosion rate decreased because of the graphene film.

In the present work, graphene contributed to the inhibition of both the anodic and cathodic reaction rates compared to annealed Cu. Remarkably, the effect was more prominent for G-Ann-20%H_2 and G-Ann-50%H_2 compared to G-Ann-2.5%H_2 and G-Ann-0%H_2 specimens, suggesting that graphene film deposited under these conditions was more stable and protective. The coating was protecting the underlying Cu surface by minimizing the movement of ionic species between the solvent and the substrate. The decrease in i_{corr} and increase in E_{corr} indicate that graphene is mainly acting as an anodic barrier for these specimens, which ultimately decreases the corrosion rate. The comparison of corrosion data, E_{corr}, i_{corr}, i_{pass} (passive current density), and E_{pit} (pitting potential), measured at − 200 mV for all specimens is given in Table 1. Data of this table show that the lowest i_{corr} was observed for G-Ann-20%H_2, indicating that this specimen has the lowest corrosion rate as confirmed by Tafel analysis.

In order to get more insight on the corrosion protection and electro-kinetic behavior of graphene-coated Cu specimens, nondestructive and conventional EIS measurements were performed in 0.5 M NaCl solution. The obtained EIS data are presented in Fig. 4a in Bode format (impedance module and phase angle vs. log (freq.)). The data are investigated using EIS fitting analysis using the equivalent circuit and displayed in Fig. 4(b), and the relevant EIS values are listed in Table 2. R_s and R_{ct} signify the electrolyte and charge transfer resistance, respectively. Constant phase element (CPE_{dl}) denotes constant phase element of the double-layer capacitance of the barrier layer. In order to achieve precise fitting results, capacitive element (C) was substituted by CPE and the impedance of a CPE is described as $Z_{CPE} = [Y_0 (j\ \omega)^n]^{-1}$, where Y_0 and n mention frequency-independent values and ω represents the angular frequency (Ref 29, 30). The value of n fluctuating from 0 to 1 has been intensely governed by the surface microstructure, where a value of 1 designates that the surface is perfect and that the impedance of the CPE is deliberated as a pure capacitor (Ref 31).

From Table 2, the R_{ct} values obtained for G-Ann specimens were comparatively higher than that of annealed Cu specimens, corresponding to the physical barrier behavior of graphene coatings (Ref 32). The G-Ann-20%H_2 specimen exhibited higher R_{ct} value (7288 × Ω cm^2) than their respective G-Ann-Cu, demonstrating the improved surface protection effectiveness of graphene layer with 20% concentration of H_2, probably owing to a strong adherent, different film morphology with less porousity in nature (Ref 33). It is evidently observed that the values of CPE_{dl} were significantly reduced due to the presence of the graphene layer which inhibited the pathway of aggressive elements from the electrolytes toward Cu surface (Ref 34). In particular, compared with the CPE_{dl} value of annealed and graphene-coated Cu specimens, G-Ann-20% specimen exhibits the lowest CPE_{dl} value (0.56 μFcm^2), indicating that the graphene layer processed under this condition possessed a stable film/Cu interface with no sign of corrosion damages. The exponent of CPE_{dl}, n_{dl}, of investigated G-Ann-Cu substrates is almost nearing to 1, indicating that graphene film processed at annealed Cu specimen was more compact with a homogeneous surface than that of annealed Cu (n_{dl}-0.91), and the enhanced barrier performance of graphene film efficiently hindered the diffusion of aggressive species from the electrolyte (Ref 35). Based on the obtained results from electrochemical corrosion studies, the surface protective behavior against corrosion provided by graphene coatings is categorized as G-Ann-20%H_2 > G-Ann-50%H_2 > G-Ann-2.5%H_2 > G-Ann-0%H_2 > G-Ann.

In summary, the corrosion results revealed that a change in H_2 concentration did affect the quality of deposited graphene which in turn affected its corrosion performance. The best results in terms of anodic/cathodic inhibition were obtained when graphene film was grown after annealing at 20 and 50%H_2 concentration, i.e., G-Ann-20%H_2 and G-Ann-50%H_2 specimens. This corrosion behavior could be correlated with the graphene characteristics and the surface morphology of underlying Cu. It is shown in Fig. 2 that graphene film varied in thickness and quality when produced at different H_2 concentrations. Depending on the annealing conditions, bilayer and multilayer graphene films were grown. Though the films produced at 0 and 2.5% of H_2 had a lower Raman D-band, however, they showed lower corrosion resistance compared to 20%H_2 specimen (Table 1). This could be understood as follows: at 0 or 2.5%H_2, mono/bilayer graphene film was obtained along with several oxide particles. In addition, Cu surface exhibited a high density of steps and thus high

Table 1 Corrosion data (measured at − 200 mV) of annealed Cu and G/Cu. The corrosion rate was estimated in millimeter per year (mpy)

Specimen	E_{corr}, mV	E_{pit}, mV	i_{corr}, μA/cm^2	i_{pass}, μA/cm^2	Corrosion rate, mpy
Ann-Cu	− 388	− 147	90.1	34	5.2035
G-Ann-0%H_2	− 335	− 180	2.81	3.8	0.1625
G-Ann-2.5%H_2	− 255	− 126	0.794	1.3	0.0459
G-Ann-20%H_2	− 239	− 80	0.15	0.18	0.0087
G-Ann-50%H_2	− 245	− 100	0.156	0.37	0.0090

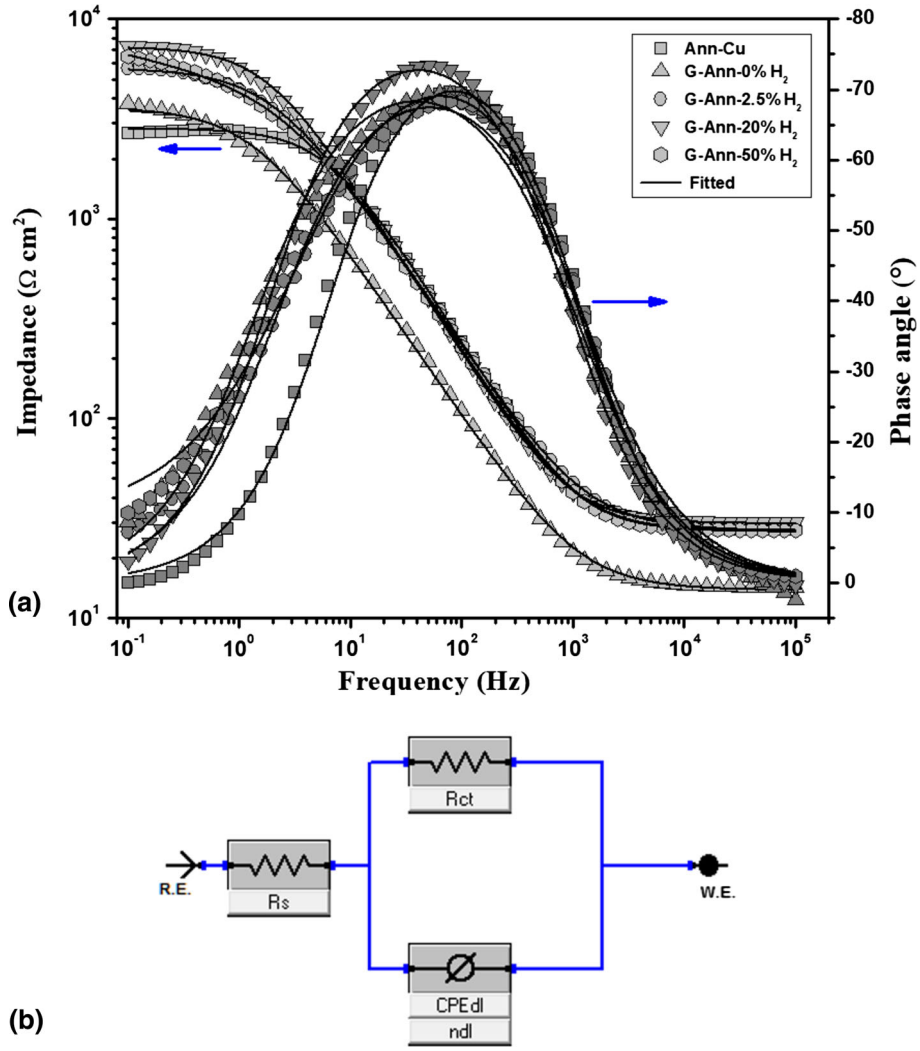

Fig. 4 Bode plots of annealed Cu and graphene-coated Cu specimens exposed in 0.5 M NaCl solution at room temperature

Table 2 EIS parameters for the annealed and graphene-coated Cu in 0.5 M NaCl solution

Specimen	R_s, Ω cm^2	Q_1, μF cm^{-2}	n_1	R_f, kΩ cm^2	Q_2, μF cm^{-2}	n_2	R_{ct}, kΩ cm^2
Ann-Cu	52.55	112.54	0.89	2.045	62.54	0.90	2.668
G-Ann-0%H_2	48.21	18.52	0.92	2.631	10.25	0.94	3.641
G-Ann-2.5%H_2	49.57	12.35	0.92	4.023	6.35	0.94	5.637
G-Ann-20%H_2	50.05	8.95	0.91	4.135	2.21	0.95	7.328
G-Ann-50%H_2	56.24	10.57	0.93	5.263	4.87	0.93	6.396

roughness (see Fig. 1e). As a result, graphene grown on such high surface features was unlikely to cover the surface completely and hence the enhancement in corrosion resistance was limited. On the contrary, multilayer graphene grown over Cu under 20 and 50%H_2 concentrations was able to decrease the corrosion rate substantially when compared with annealed Cu. In this case, the Cu surface was smooth without any steps as displayed by AFM images (Fig. 1g and h). The graphene grown on such surfaces had better coverage and uniformity, and hence better protection against corrosion as dictated by Tafel analysis (Table 1).

3.4 Surface Morphological Analysis of Corroded Specimens

To observe the corrosion effects, optical micrographs and Raman spectra of the annealed Cu and four G/Cu specimens (G-Ann-0%H_2, G-Ann-2.5%H_2, G-Ann-20%H_2, and G-Ann-50%H_2) were captured before and after the potentiodynamic test as shown in Fig. 5. After corrosion tests, the Raman spectra of the corroded specimens at different regions were also taken, and the results of all G/Cu specimens are shown in Fig. 5(i), (j), (k), and (l). No major difference in surface morphology of G/Cu specimens was observed before the corrosion test (Fig. 5a, b, c, and d). However, the Cu surface exhibited a totally

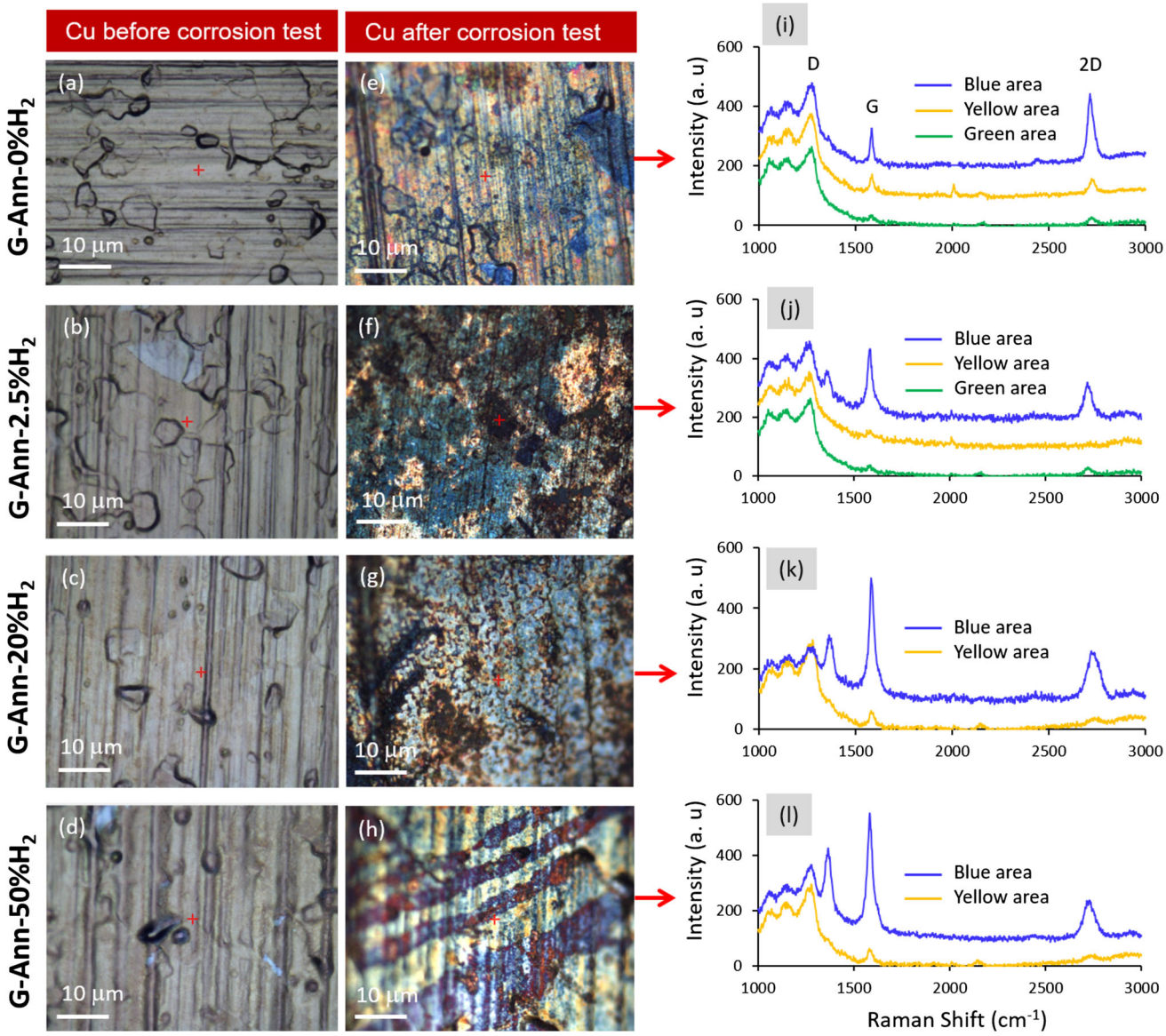

Fig. 5 Surface topography of Cu substrate and graphene film characteristics after corrosion experiments. Optical microscopy (1000 ×) of G/Cu specimens (a–d) before and (e–h) after potentiodynamic test. The topological images of Cu are showing the obvious corrosion effects after corrosion test as depicted by different colors. The corresponding Raman spectra of the specimens (i–l). The spectra were extracted by selecting an area on each color and thereafter represented with that color. The blue area in each specimen is showing the characteristic features, D, G and 2D bands of graphene. Note: The Raman spectra of the specimens (a–d) are shown in Fig. 2(a)

different morphology and colors after corrosion tests as shown in Fig. 5(e), (f), (g), and (h). Corrosion effects were seen on all four specimens with some differences. The common colors were blue, yellow, and green. The blue color was dominating in case of G-Ann-50%H_2 specimen, and bands of blue color were seen along with yellow traces. Raman spectra on each color (of specimens e-h) were taken to find out the presence of graphene (if any) after corrosion test, as shown in Fig. 5(i) and (l). The blue regions in each specimen showed the characteristic features of graphene, D, G, and 2D bands, indicating that graphene was present in this region even after the electrolyte test. On the other hand, the graphene peaks of the Raman spectra disappeared or showed negligible intensities at green and yellow regions (see green and yellow spectra), suggesting that the graphene was detached from these regions during the attack of corrosion species. The additional peaks in the range of 1000-1300 cm^{-1} were attributed to the fluorescence of Cu (Ref 36).

The surface morphology of the corroded G/Cu samples was also examined by SEM. Figure 6 shows the SEM micrographs at two magnifications of the graphene-coated Cu specimens after electrochemical tests. Note, the same specimens are shown in Fig. 1(a), (b), (c), and (d) before corrosion experiments. The Cu surface clearly demonstrated the pronounced corrosion when graphene films were grown at low H_2 concentration. The G-Ann-0%H_2 specimen severely corroded as evident by the cracks and corrosion pits; both small and deep pits were observed suggesting that the graphene film was not continuous due to Cu-stepped structure. The occurrence of deep pit sites (white arrowhead) is attributed to the discontinuous graphene layer thus allowing the electrolyte to pass through it. The G-Ann-2.5%H_2 specimen showed a little better protection but its

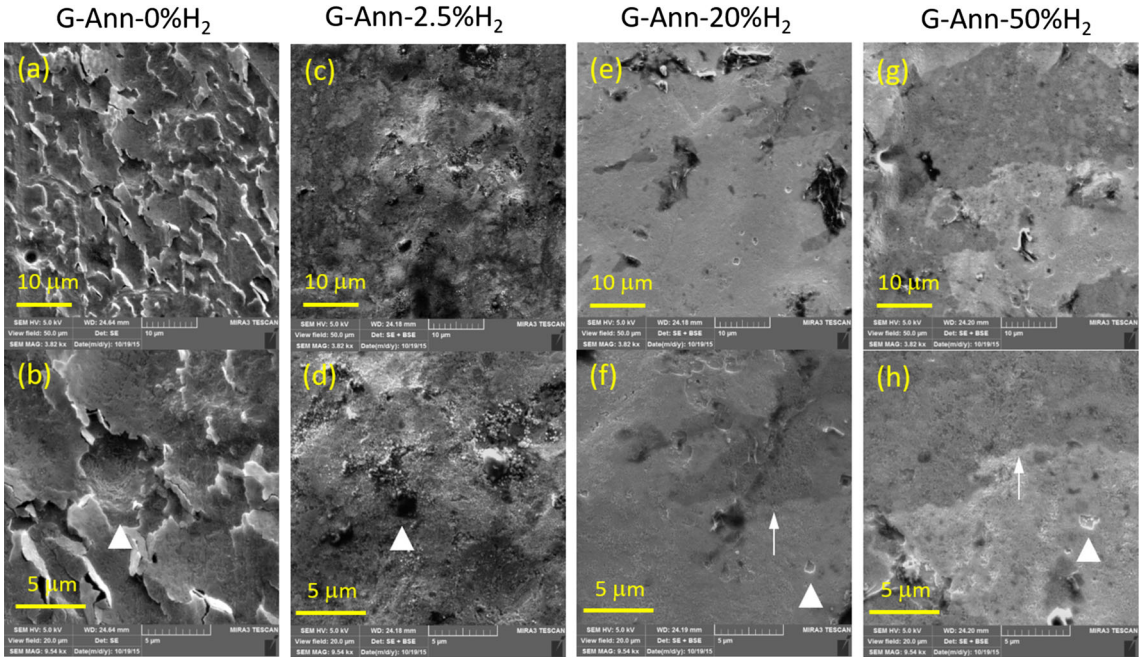

Fig. 6 Surface morphology of Cu substrate after corrosion tests. SEM micrographs of the corroded surfaces at two magnifications; (a, c, e, g) large area and (b, d, f, h) close-up view of the specimens after corrosion tests. The surface of the G-Ann-0%H_2 specimen was severely damaged compared to other specimens due to attack of corrosion species

surface was yet completely perturbed. This little improvement in the corrosion performance was attributed to uniform coverage of the graphene due to the smoother surface of Cu produced under 2.5%H_2. In contrast, G-Ann-20%H_2 and G-Ann-50%H_2 specimens showed better protection against corrosion. Only few localized corrosion sites were distributed on the surface (Fig. 6f and h), indicating that the Cu surface was well-covered and protected by a graphene film. These SEM images further support the corrosion results shown in Fig. 3, confirming that Cu with multilayer graphene exhibits a better corrosion performance.

The better corrosion performance of G-Ann-20%H_2 and G-Ann-50%H_2 specimens is ascribed by two factors which are closely linked to each other, i.e., smooth surface of the Cu and the growth of multilayer graphene. The smooth surface that is absence of Cu-stepped structure, and larger Cu grains are beneficial for the growth of a uniform layer of graphene. The multilayer graphene reduces the passage of corrosion species considerably, and hence the corrosion rate, as reflected in the electrochemical results as given in Table 1. Graphene deposition improves the corrosion resistance of Cu, such that the corrosion rate of Cu (Ann-Cu) is 5.2035 mpy, while the coated specimen (G-Ann-20%H_2) results in 0.0087 mpy, nearly three orders of magnitude slower than the annealed Cu. Comparing the coated specimens with uncoated ones, the surface morphology of the bare Cu (without graphene) was also evaluated by SEM before and after corrosion experiments (Fig. 7). The surface of Cu severely corroded after being subjected to corrosion species. The untouched Cu showed a smooth surface with some grains.

3.5 Corrosion Mechanism

The possible corrosion mechanism is shown in Fig. 8. SEM and AFM analyses reveal that Cu exhibits a rough surface when annealed under zero and/or low H_2 content during the annealing process, while showing a smooth surface at higher H_2 concentrations (20 and 50%H_2). Single-layer graphene (SLG) is obtained for Cu annealed at low H_2 concentration (0 and 2.5%H_2), as shown in Fig. 8(a). Graphene on such Cu surface could not have a uniform coverage (but rather a partial coverage) due to the presence of high surface features, e.g., Cu-stepped structure, hillocks, and grain boundaries. For such specimens, the corrosion species follow the straight path through the graphene and attack the surface of Cu. On the other hand, multilayer (4-5 layers) graphene is obtained when Cu is annealed under 20 and 50%H_2 during the annealing process. The corrosion species follow the zigzag path through multilayer graphene (MLG) domains when subjected to corrosion electrolyte. The corrosion species take more time than the former specimens to reach the surface of Cu (Fig. 8b). Thus, the corrosion rate is slower, implyingan improved corrosion performance of Cu for MLG than the SLG specimens.

4. Conclusion

In this work, we deposited graphene films of different thicknesses (bilayer and multilayer) on Cu substrate and investigated the corrosion performance of graphene/Cu in chloride ions solution, 0.5 M sodium chloride, a concentration of salt close to that of sea water. The graphene was grown by altering hydrogen (H_2) concentration during the annealing stage using CVD technique. The surface morphological features of graphene/Cu were examined by SEM and AFM. SEM and AFM results clearly highlighted the variation of graphene thickness and roughness of Cu surface obtained under different H_2 concentration. At 20 and 50% H_2 concentrations, 4-5 layers of graphene were obtained as confirmed by Raman

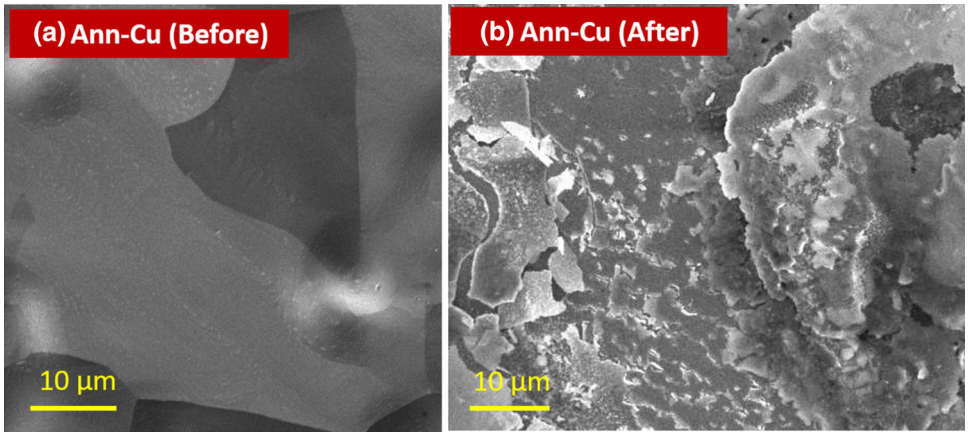

Fig. 7 SEM micrographs of the bare Cu (a) before and (b) after potentiodynamic tests. The surface of the Cu was severely damaged after corrosion

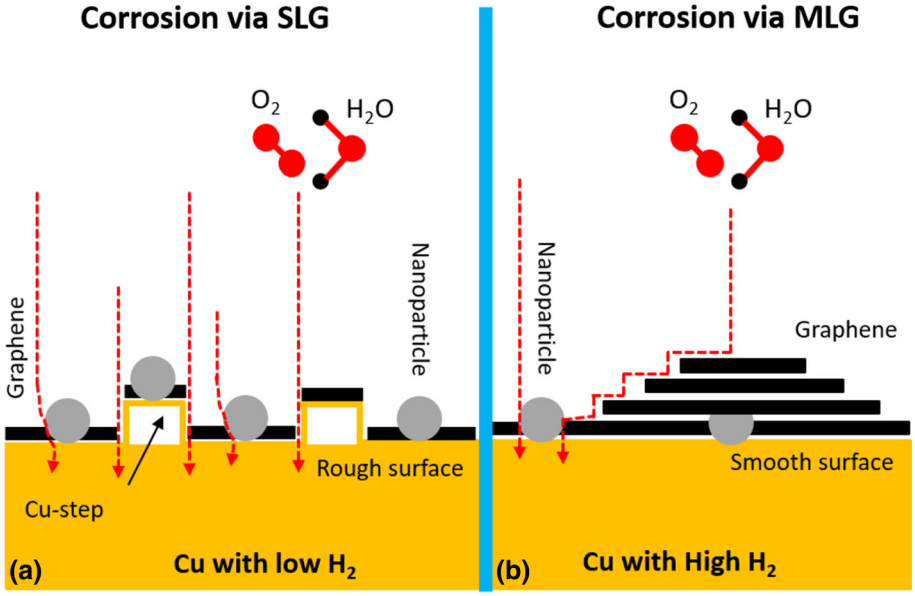

Fig. 8 Schematic representation of corrosion species (O_2 and H_2O) following (a) a straight path through single/bilayer graphene (SLG) domains; (b) and tortuous path through multilayer graphene (MLG) domains. Cu exhibits rough surface when annealed under zero/low H_2 while smooth surface if annealed at high H_2 concentrations (20 and 50%H_2)

spectroscopy and TEM analysis. These graphene films offered the best corrosion protection against electrochemical degradation. By Tafel analysis, it was found that the corrosion rate of G-Ann-20%H_2 specimen was nearly three orders of magnitude lower than that of annealed Cu. The results obtained in this study suggest that corrosion properties of graphene/metal can be improved by optimizing CVD conditions and tailored for specific applications where resistance to salt is an important factor.

Acknowledgments

The authors acknowledge the support provided by King Fahd University of Petroleum and Minerals in Dhahran, and that of the IMRC administration at Imam Abdulrahman Bin Faisal University in Dammam, Saudi Arabia, as well as that of University of Sharjah, United Arab Emirates.

Conflict of interest

The authors declare that they have no conflict of interest.

References

1. B.P. Singh et al., The Production of a Corrosion Resistant Graphene Reinforced Composite Coating on Copper by Electrophoretic Deposition, *Carbon*, 2013, **61**, p 47–56
2. V.K. Mittal et al., Formation and Characterization of Bi-layer Oxide Coating on Carbon-Steel for Improving Corrosion Resistance, *Thin Solid Films*, 2009, **517**(5), p 1672–1676
3. Y. Chen et al., Fabrication and Anti-corrosion Property of Superhydrophobic Hybrid Film on Copper Surface and Its Formation Mechanism, *Surf. Interface Anal.*, 2009, **41**(11), p 872–877
4. J.S. Bunch et al., Impermeable Atomic Membranes from Graphene Sheets, *Nano Lett.*, 2008, **8**(8), p 2458–2462
5. O. Leenaerts, B. Partoens, and F.M. Peeters, Water on Graphene: Hydrophobicity and Dipole Moment Using Density Functional Theory, *Phys. Rev. B*, 2009, **79**(23), p 235440

6. T. Kim, S. Lee, and H. Park, A Study of Water Transport as a Function of the Micro-Porous Layer Arrangement in PEMFCs, *Int. J. Hydrog. Energy*, 2010, **35**(16), p 8631–8643
7. N.T. Kirkland et al., Exploring Graphene as a Corrosion Protection Barrier, *Corros. Sci.*, 2012, **56**, p 1–4
8. C. Liang et al., Hydrogen Etching Effect on Single-Crystal Graphene Domains. In: 2013 8th Annual IEEE International Conference on Nano/Micro Engineered and Molecular Systems (IEEE NEMS 2013), 2013: p 697–700
9. D. Prasai et al., Graphene: Corrosion-Inhibiting Coating, *ACS Nano*, 2012, **6**(2), p 1102–1108
10. R.K.S. Raman et al., Protecting Copper from Electrochemical Degradation by Graphene Coating, *Carbon*, 2012, **50**(11), p 4040–4045
11. Y.H. Dong, Q.Q. Liu, and Q. Zhou, Corrosion Behavior of Cu during Graphene Growth by CVD, *Corros. Sci.*, 2014, **89**, p 214–219
12. A. Reina et al., Large Area, Few-Layer Graphene Films on Arbitrary Substrates by Chemical Vapor Deposition, *Nano Lett.*, 2009, **9**(1), p 30–35
13. Y.Q. Liang et al., Large-Scale Synthetic Graphene on Cu as Anti-Corrosion Coating by Chemical Vapor Deposition Approach, *Sci. Adv. Mater.*, 2014, **6**(3), p 545–549
14. A. Ibrahim et al., Effects of Annealing on Copper Substrate Surface Morphology and Graphene Growth by Chemical Vapor Deposition, *Carbon*, 2015, **94**, p 369–377
15. W. Liu et al., Synthesis of High-Quality Monolayer and Bilayer Graphene on Copper Using Chemical Vapor Deposition, *Carbon*, 2011, **49**(13), p 4122–4130
16. H. Kim et al., Activation Energy Paths for Graphene Nucleation and Growth on Cu, *ACS Nano*, 2012, **6**(4), p 3614–3623
17. H. Wang et al., Controllable Synthesis of Submillimeter Single-Crystal Monolayer Graphene Domains on Copper Foils by Suppressing Nucleation (vol 134, pg 3627, 2012), *J. Am. Chem. Soc.*, 2012, **134**(44), p 18476–18476
18. S. Bhaviripudi et al., Role of Kinetic Factors in Chemical Vapor Deposition Synthesis of Uniform Large Area Graphene Using Copper Catalyst, *Nano Lett.*, 2010, **10**(10), p 4128–4133
19. Y.C. Shin and J. Kong, Hydrogen-Excluded Graphene Synthesis via Atmospheric Pressure Chemical Vapor Deposition, *Carbon*, 2013, **59**, p 439–447
20. L. Gan and Z.T. Luo, Turning Off Hydrogen to Realize Seeded Growth of Subcentimeter Single-Crystal Graphene Grains on Copper, *ACS Nano*, 2013, **7**(10), p 9480–9488
21. Z.J. Wang et al., Direct Observation of Graphene Growth and Associated Copper Substrate Dynamics by In Situ Scanning Electron Microscopy, *ACS Nano*, 2015, **9**(2), p 1506–1519
22. X.F. Zhang et al., Hydrogen-Induced Effects on the CVD Growth of High-Quality Graphene Structures, *Nanoscale*, 2013, **5**(18), p 8363–8366
23. D.H. Jung et al., Effects of Hydrogen Partial Pressure in the Annealing Process on Graphene Growth, *J. Phys. Chem. C*, 2014, **118**(7), p 3574–3580
24. J. Song, T.Y. Ko, and S. Ryu, Raman Spectroscopy Study of Annealing-Induced Effects on Graphene Prepared by Micromechanical Exfoliation, *Bull. Korean Chem. Soc.*, 2010, **31**(9), p 2679–2682
25. Z.Z. Sun et al., Growth of Graphene from Solid Carbon Sources, *Nature*, 2010, **468**(7323), p 549–552
26. X.C. Dong et al., Growth of Large-Sized Graphene Thin-Films by Liquid Precursor-Based Chemical Vapor Deposition under Atmospheric Pressure, *Carbon*, 2011, **49**(11), p 3672–3678
27. J.C. Meyer et al., The Structure of Suspended Graphene Sheets, *Nature*, 2007, **446**(7131), p 60–63
28. E. Widenkvist et al., Mild Sonochemical Exfoliation of Bromine-Intercalated Graphite: A New Route Towards Graphene, *J. Phys. D Appl. Phys.*, 2009, **42**, p 112003
29. A. Madhankumar et al., EIS Evaluation of Protective Performance and Surface Characterization of Epoxy Coating with Aluminum Nanoparticles After Wet and Dry Corrosion Test, *J. Solid State Electrochem.*, 2012, **16**(6), p 2085–2093
30. S. Akhtar et al., Enhancement of Anticorrosion Property of 304 Stainless Steel Using Silane Coatings, *Appl. Surf. Sci.*, 2018, **440**, p 1286–1297
31. A.V. Benedeti et al., Electrochemical Studies of Copper, Copper-Aluminium and Copper-Aluminium-Silver Alloys: Impedance Results in 0.5 M NaCl, *Electrochim. Acta*, 1995, **40**(16), p 2657–2668
32. P.G. Pawar et al., Polystyrene Assisted Superhydrophobic Silica Coatings with Surface Protection and Self-Cleaning Approach, *Prog. Org. Coat.*, 2017, **105**, p 235–244
33. A.Y. Adesina, Z.M. Gasem, and A.M. Kumar, Corrosion Resistance Behavior of Single-Layer Cathodic Arc PVD Nitride-Base Coatings in 1 M HCl and 3.5 pct NaCl Solutions, *Metall. Mater. Trans. B*, 2017, **48**(2), p 1321–1332
34. A.M. Kumar et al., Fabrication of Nitrogen Doped Graphene Oxide Coatings: Experimental and Theoretical Approach for Surface Protection, *RSC Adv.*, 2015, **5**(25), p 19264–19272
35. A.M. Kumar et al., Promising Hard Carbon Coatings on Cu Substrates: Corrosion and Tribological Performance with Theoretical Aspect, *J. Mater. Eng. Perform.*, 2018, **27**(5), p 2306–2316
36. S.D. Costa et al., Resonant Raman Spectroscopy of Graphene Grown on Copper Substrates, *Solid State Commun.*, 2012, **152**(15), p 1317–1320